Since January 2020 Elsevier has created a COVID-19 resource centre with free information in English and Mandarin on the novel coronavirus COVID-19. The COVID-19 resource centre is hosted on Elsevier Connect, the company's public news and information website.

Virology 575 (2022) 91–100

Contents lists available at ScienceDirect

Virology

journal homepage: www.elsevier.com/locate/virology

Estimation of virus-mediated cell fusion rate of SARS-CoV-2

Ava Amidei [a], Hana M. Dobrovolny [b,*]

[a] Department of Chemistry & Biochemistry, Texas Christian University, Fort Worth, TX, USA
[b] Department of Physics & Astronomy, Texas Christian University, Fort Worth, TX, USA

ARTICLE INFO

Keywords:
Mathematical modelling
Syncytia formation
Fusion rate
ACE2 receptor
Furin
TMPRSS2
Spike protein

ABSTRACT

Several viruses have the ability to form large multinucleated cells known as syncytia. Many properties of syncytia and the role they play in the evolution of a viral infection are not well understood. One basic question that has not yet been answered is how quickly syncytia form. We use a novel mathematical model of cell-cell fusion assays and apply it to experimental data from SARS-CoV-2 fusion assays to provide the first estimates of virus-mediated cell fusion rate. We find that for SARS-CoV2, the fusion rate is in the range of 6×10^{-4}–12×10^{-4}/h. We also use our model to compare fusion rates when the protease TMPRSS2 is overexpressed (2–4 times larger fusion rate), when the protease furin is removed (one third the original fusion rate), and when the spike protein is altered (1/10th the original fusion rate). The use of mathematical models allows us to provide additional quantitative information about syncytia formation.

1. Introduction

In 2019, a novel coronavirus, SARS-CoV-2, was identified in Wuhan, China and rapidly spread around the world (Chen et al., 2020; Wu et al., 2020). The virus has a range of effects, from asymptomatic infection (Syangtan et al., 2021) to severe illness and death (Sun et al., 2020; Goyal et al., 2020; Jiang et al., 2020). While much has been learned about the virus and it's infection dynamics within the human body over the last two years (Hakim et al., 2021), there are some aspects of virus-host interaction that remain unclear. In particular, the mechanistic links between severity of the disease, tissue damage, and viral load are still not understood (Acer et al., 2022; Simons et al., 2022; El Jamal et al., 2021).

One possible contributor to both damage and disease severity is the formation of multinucleated cells known as syncytia. SARS-CoV-2 is known to have the ability to form syncytia (Braga et al., 2021; Barreto-Vieira et al., 2022; Hoffmann et al., 2020) that can contribute to disease severity in a number of ways. The formation of syncytia causes physical tissue damage that results in more severe clinical symptoms (Bussani et al., 2020). Additionally, the formation of syncytia has been shown to initiate the cGAS-STING signaling pathway that can induce an aberrant immune response (Ren et al., 2021), perhaps contributing to severe cases of COVID-19. The syncytia have also been shown to internalize lymphocytes (Zhang et al., 2021a), preventing them from responding to the infection.

A number of experimental studies have started examining the fusion process in more detail in an attempt to identify processes that control the rate of fusion. Studies have found that syncytia formation was inhibited by interferon-induced transmembrane proteins (Buchrieser et al., 2020) and enhanced by the presence of the proteases TMPRSS2 (Buchrieser et al., 2020; Hoernich et al., 2021; Papa et al., 2021) or furin (Papa et al., 2021). Sanders et al. determined that cholesterol-rich regions of the membrane are particularly susceptible to fusion (Sanders et al., 2021). Fusogenicity has been linked to several different changes in the spike protein. One study noted that the D614G substitution on the spike protein increases syncytia formation (wen Cheng et al., 2021) while other studies found that removal of the ER-retention motif or modification of the spike protein cleavage site reduce the fusogenicity of the virus (Wang et al., 2021; Papa et al., 2021). Another study examined the quasispecies of SARS-CoV-2 produced during an infection and noted a high frequency of a deletion mutation (SΔ20) on the spike protein that increased the ability of the virus to form syncytia. Finally, a study of syncytia formation of different SARS-CoV-2 variants suggests that the more recent SARS-CoV-2 alpha, beta, and delta variants are more fusogenic than the original Wuhan strain (Rajah et al., 2021).

While some of these studies have made quantitative comparisons of the amount of fusion or the number of syncytia (Buchrieser et al., 2020; Sanders et al., 2021; Papa et al., 2021; Rajah et al., 2021), this might not provide the best assessment of the overall fusogenicity of the virus. A modification to the spike protein or to the cell receptors that causes

* Corresponding author.
E-mail address: h.dobrovolny@tcu.edu (H.M. Dobrovolny).

https://doi.org/10.1016/j.virol.2022.08.016
Received 19 July 2022; Received in revised form 27 August 2022; Accepted 28 August 2022
Available online 7 September 2022

fusion to occur more slowly might still result in more overall tissue damage, but this effect will not be captured by measuring the number of syncytia at a specific, usually early, time. A better assessment of the fusogenicity of a virus or a particular viral strain would be to estimate the rate of virus-mediated cell fusion. Experimentally, fusion rate is difficult to measure directly, but it can be estimated through the use of mathematical models.

While the use of mathematical models to study the role of syncytia in viral infections is still limited (Jessie and Dobrovolny, 2021; Alzahrani et al., 2020), mathematical modeling has been used to estimate other viral kinetics parameters for a variety of viruses (Baccam et al., 2006; González-Parra and Dobrovolny, 2015; González-Parra et al., 2018; Liao et al., 2020; Hernandez-Vargas and Velasco-Hernandez, 2020; Rezelj and Vignuzzi, 2020). Parameter estimates have then been used to compare a variety of scenarios, such as the effect of a particular mutation (Pinilla et al., 2012; Paradis et al., 2015; Simon et al., 2016; Petrie et al., 2015), the effect of treatment (Dobrovolny, 2020) or aging (Wethington et al., 2019; Khan et al., 1080; Rodriguez and Dobrovolny, 2021; González-Parra and Dobrovolny, 2018). Not only do these quantitative comparisons help us understand the effect of different changes, the parameter estimates can point to mechanistic changes that can be further explored with mathematical models.

In this manuscript, we fit a mathematical model to data from cell fusion assays described in (Papa et al., 2021) to both estimate a virus-mediated cell fusion rate, but to also quantitatively assess how the fusion rate is affected by availability of proteases or modification of the SARS-CoV-2 spike protein. In the absence of any changes to proteases or the spike protein, we find a fusion rate in the range of 6×10^{-4}–12×10^{-4}/h. We find that the enhanced expression of TMPRSS2 on acceptor cells increases the fusion rate while removal of furin on donor cells decreases the fusion rate. Finally, altering the spike cleavage site results in the largest decrease in the fusion rate.

2. Methods

2.1. Donor-acceptor cell fusion assay

The experimental data used in this manuscript was digitized from Papa et al. (2021); for full experimental details see (Papa et al., 2021). The cell-cell fusion assays start with two types of cells: donors and acceptors. The donor cell is co-transfected with the SARS-CoV-2 spike protein and pmCherry-N1. The pmCherry-N1 causes donor cells to fluoresce in red. The acceptor cell expresses the ACE2 receptor and is stained with Cell-TrackerTM Green CMFDA to fluoresce in green. Both donor and acceptor cells are seeded at 70% confluency in 24 multiwell plates for transfection and/or staining. To allow sufficient time for expression of proteins, cells are incubated for 5 h after transfection. At this time, donor cells are detached and mixed with acceptor cells, then the mixture is plated onto 12 multiwell plates. Fluorescence is measured at several time points over 36 or 66 h with fused cells fluorescing in orange.

The cell-cell fusion assay was used to assess the effect of several biological conditions:

- **Effect of cell type:** Both Vero cells and HEK293T cells were used as donors and acceptors to verify that it was expression of surface proteins that mediated cell fusion.
- **Effect of TMPRSS2:** TMPRSS2 is a protease that has been shown to aid in the cleavage of the SARS-CoV-2 spike protein (Takeda, 2022), thereby enabling fusion of the virus to cells, and in these experiments, enabling cell-cell fusion. Both Vero and HEK293T cells were transfected to over-express TMPRSS2 to assess the effect of this protease (Vero+TMPRSS2 or 293+TMPRSS2). In another version of these experiments, TMPRSS2 knockout cells were created that did not express TMPRSS2 (293-TMPRSS2).
- **Effect of furin:** Furin is another protease thought to aid in the cleavage of the SARS-CoV-2 spike protein (Zhang et al., 2021b). To assess the effect of furin, Vero and HEK293T furin knock-out cells were created.
- **Change in the spike cleavage site:** Both TMPRSS2 and furin cleave the spike protein at similar locations. A modified spike protein was created with this cleavage site replaced so that neither protease could cleave the spike protein. Cells expressing a modified spike protein are denoted with 'GSAS', which is the amino acid substitution placed at the RRAR site.

Table 1 contains a list of all the combinations of donor and acceptor cells assessed in (Papa et al., 2021) and the corresponding figure and curve containing the data for that case.

2.2. Mathematical models

The data in Papa et al. (2021) consists of the fraction of area in a layer of cells containing syncytia. A simplified model of syncytia formation for this system is given by

$$\begin{aligned}\frac{dD}{dt} &= -\gamma DA\\ \frac{dA}{dt} &= -\gamma DA - \gamma SA\\ \frac{dS}{dt} &= 2\gamma DA + \gamma SA.\end{aligned} \tag{1}$$

Here, donor cells, D, that are expressing the spike protein can bind with acceptor cells, A, to form syncytia S. Note that S represents the number of cells in the syncytia, not the number of syncytia. Already formed syncytia can add additional cells by binding to acceptor cells. The syncytia formation rate is γ. We assume that each cell occupies the same area, so converting to area will result in a common multiplicative factor in all terms of the equation that will simply cancel out.

We also investigate (in the Supplementary Material) a more symmetric model where both donor and acceptor cells can bind to already formed syncytia. This would appear to be the more realistic model of the processes occurring during the experiment. After all, syncytia should be expressing both the spike protein and the ACE2 receptors, so should have the ability to fuse with either donor or acceptor cells, but we found that this model does not fit the data as well as the model where only acceptor cells can bind to existing syncytia (see Supplementary Material). This could be because syncytia express more of the spike protein

Table 1
Combinations of donor and acceptor cells and the figures in (Papa et al., 2021) that contain the corresponding data.

Donor cell	Acceptor Cell	Figure	Line/Symbol
Vero	Vero	1D	Black circles
Vero	293	1D	Lavender circles
293	Vero	1D	Cyan squares
Vero	293+TMPRSS2	1D	Cyan/grey circles
293	Vero+TMPRSS2	1D	Orange squares
293	Vero	3C	Purple circles
293-furin	Vero	3C	Teal circles
293-GSAS	Vero	3C	Blue circles
293-furin-GSAS	Vero	3C	Orange circles
293	Vero	3E	Black squares
293	Vero-furin	3E	Pink squares
293-furin	Vero	3E	Teal circles
293-furin	Vero-furin	3E	Purple circles
293-GSAS	Vero	3E	Violet triangles
293-GSAS	Vero-furin	3E	Cyan triangles
293-GSAS-furin	Vero	3E	Black triangles
293-GSAS-furin	Vero-furin	3E	Pink triangles
Vero	293	5C	Navy circles
Vero	293-TMPRSS2	5C	Purple squares
Vero-GSAS	293	5C	Rose triangles
Vero-GSAS	293-TMPRSS2	5C	Magenta triangles

for some reason or because the ODE model is not adequately capturing the spatial heterogeneity of the system. Both models can be solved analytically and mathematical analysis is included in the Supplementary Material.

2.3. Model fitting procedure

Data is extracted from the figures using WebPlotDigitizer (www.webplotdigitizer.com). Models are fit to data by minimizing the sum of squared residuals (SSR) to estimate two free parameters. The first free parameter is the fusion rate γ. The second free parameter is the initial fraction of donor cells ($D(0)$). For the fits described in the main manuscript, we assume that cells cover the entire surface area, i.e. $D(t) + A(t) + S(t) = 100$. If we assume that there are initially no syncytia ($S(0) = 0$), then we must have $A(0) = 100 - D(0)$.

In the Supplementary Material, we also explore fits under the assumption that the cells do not necessarily cover the entire surface area. This requires an extra parameter to be fit: the total covered surface area (T). In this case, we still assume that the initial number of syncytia is zero, so our constraint becomes $A(0) = T - D(0)$.

Posterior distributions for the parameter estimates are determined using 1000 bootstrap replicates (Efron and Tibshirani, 1986). The Mann-Whitney test is used to test for statistical differences between distributions for the fusion parameter estimate. This test does not require an assumption of normal distributions. To avoid overpowering, 100 random samples of 10 estimates are pulled from each distribution to perform the statistical comparison and the mean p value is presented.

3. Results

3.1. Effect of cell type

One series of experiments examined whether the cell type used as donor or acceptor changed the results of the experiment. Fig. 1 shows the experimental time courses along with model fits for these experiments (top row) and the resulting distributions for the fusion rates in the three cases (bottom row). Parameter values for the fits are given in Table 2. Correlation plots and likelihood profiles are included in the Supplementary Material.

We find fusion rates of 7.73×10^{-4}/h (95% CI (6.65–9.40) $\times$ 10^{-4}/h) for the Vero/Vero combination; 9.62×10^{-4}/h (95% CI (7.07–12.0) $\times$ 10^{-4}/h) for the Vero/293 combination; and 8.85×10^{-4}/h (95% CI (6.78–11.3) $\times$ 10^{-4}/h) for the 293/Vero combination. The distributions for the estimated fusion rates for all three cases overlap substantially and there is no statistically significant difference between the distributions as assessed by the Mann-Whitney test ($p = 0.030$ for the Vero/Vero and Vero/293 distributions; $p = 0.15$ for the Vero/Vero and 293/Vero distributions; and $p = 0.36$ for the Vero/293 and 293/Vero distributions).

Table 2
Best fit parameter values for experiments with different cell types.

Experiment	Fusion rate (/hour)	Initial percentage of donors	SSR
Vero/Vero	7.73 (6.65–9.40)$\times$ 10^{-4}	17.7 (11.7–30.3)	56.2 (2.98–108)
Vero/293	9.62 (7.07–12.0)$\times$ 10^{-4}	7.08 (3.79–14.7)	122 (14.7–168)
293/Vero	8.85 (6.78–11.3)$\times$ 10^{-4}	10.9 (6.02–21.7)	124 (6.11–208)

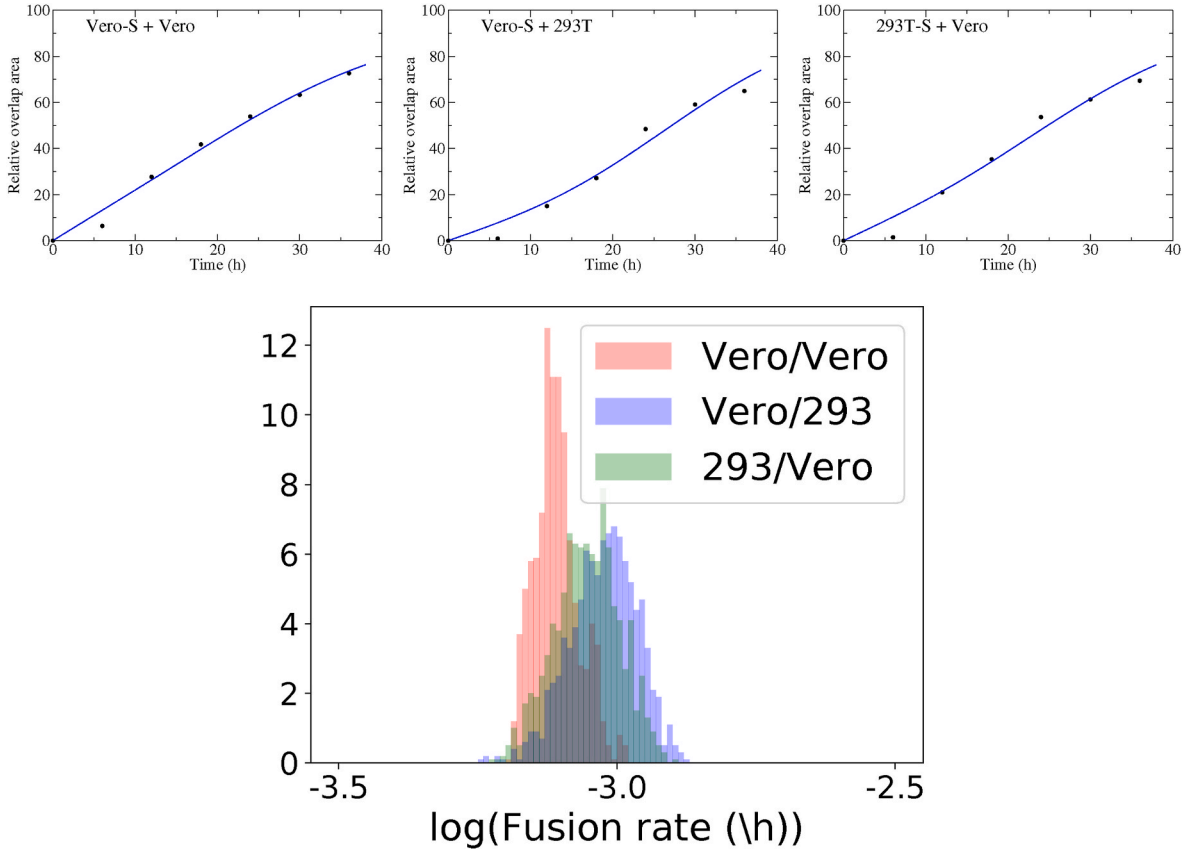

Fig. 1. Dependence of fusion rate estimates on cell type. Top row shows the experimental time courses of Vero/Vero fusion (left) and Vero/293 fusion (center) and 293/Vero (right) along with model best fit curves. Bottom figure shows the distributions of fusion rate estimates for each case.

Thus the cell type used as the basis for donor or acceptor cell does not appear to affect the fusion rate.

The model fitting also provides an estimate of the initial percentage of donors (Table 2). We note that the estimated initial percentage of donors is small considering that the experimental protocol suggests that there should initially be a fairly even mix of donors and acceptors. As shown in the Supplementary Material (Fig. S5), the asymmetric model can capture a plateau in the area covered by syncytia of less than 100% by adjusting the initial fraction of donors and acceptors. Thus the low estimates of initial percentage of donor cells are reflecting the low plateau of the syncytia, rather than an actual skewed ratio of donor and acceptor cells.

3.2. Effect of TMPRSS2

Experiments to study the effect of TMPRSS2 were performed in two combinations of donor/acceptor cells. The Vero/293 combination was tested with the acceptor both over-expressing TMPRSS2 (Vero/293+TMPRSS2) and the acceptor having TMPRSS2 knocked out (Vero/293-TMPRSS2). The 293/Vero combination was tested only with acceptor cells over-expressing TMPRSS2 (293/Vero+TMPRSS2). Fig. 2 shows the experimental time courses of the data sets used in this analysis along with model best fits. The estimated fusion rate distributions are shown in the bottom row of Fig. 2. Best fit parameter estimates are given in Table 3 while correlation plots and likelihood profiles are given in the Supplementary Material.

The model fits for the fusion experiments with cells over-expressing TMPRSS2 do not quite capture the height of the plateau present in the experimental data. The Supplementary Material explores extensions to the model and fitting methodology that help correct this issue. For the Vero/293 combination, we find a fusion rate of 2.31×10^{-3}/h (95% CI

Table 3
Best fit parameter values for experiments examining the effect of TMPRSS2.

Experiment	Fusion rate (/hour)	Initial percentage of donors	SSR
Vero/293	9.62 (7.07–12.0)×10^{-4}	7.08 (3.79–14.7)	122 (14.7–168)
Vero/293+TMPRSS2	2.31 (1.79–3.50)×10^{-3}	3.26 (0.702–8.98)	393 (57.0–537)
Vero/293-TMPRSS2	1.23 (0.713–2.15)×10^{-3}	92.1 (90.4–93.1)	15.5 (1.73–25.1)
293/Vero	8.85 (6.78–11.3)×10^{-4}	10.9 (6.02–21.7)	124 (6.11–208)
293/Vero+TMPRSS2	3.96 (2.88–7.47)×10^{-3}	1.10 (0.0133–4.70)	653 (231–757)

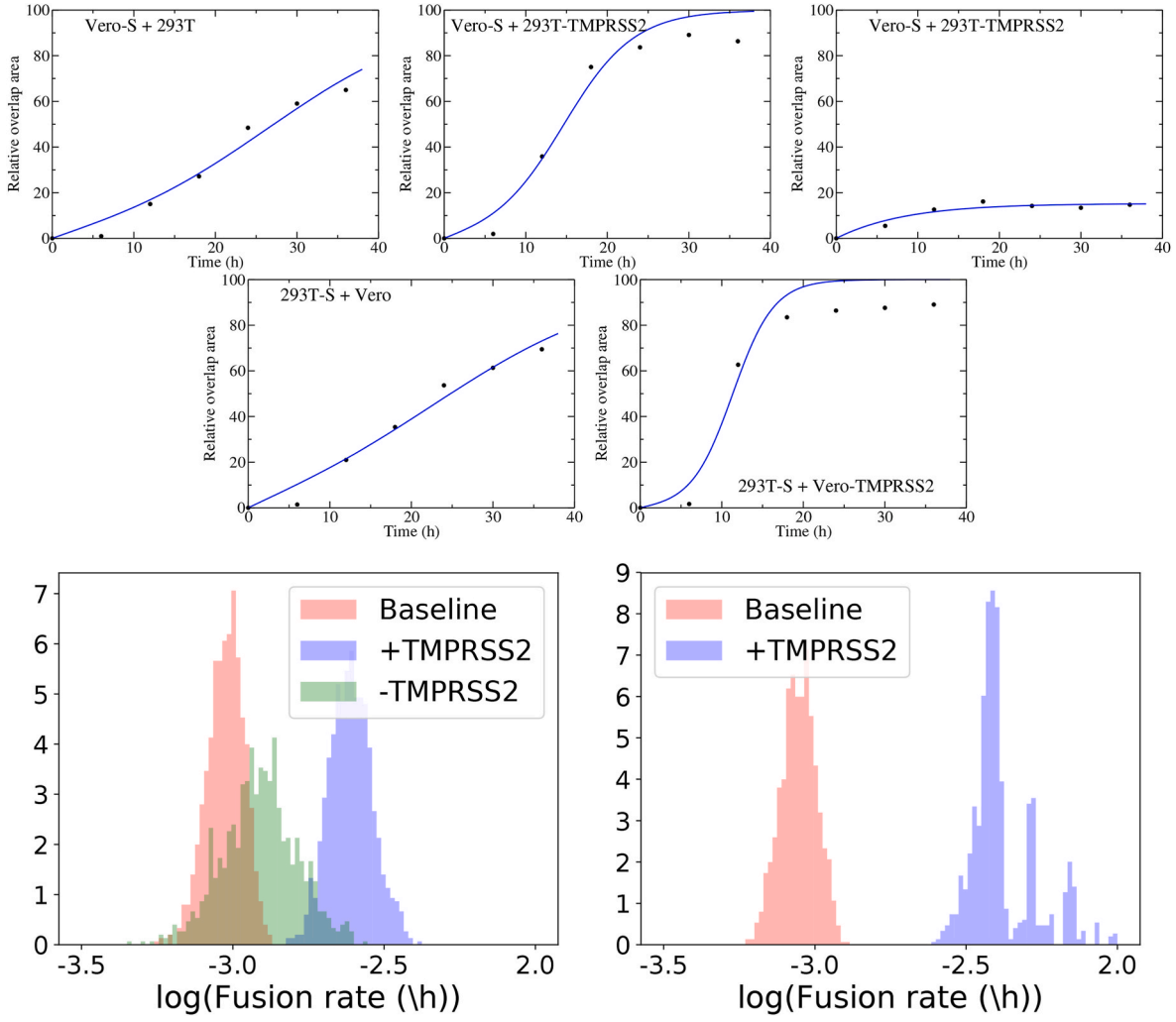

Fig. 2. Dependence of fusion rate estimates on TMPRSS2. Top row shows the experimental time courses of Vero/293 fusion (left) and Vero/293+TMPRSS2 fusion (center) and Vero/293-TMPRSS (right) along with model best fit curves. Center row shows the experimental time courses and model fits for 293/Vero fusion (left) and 293/Vero+TMPRSS2 fusion (right). Recall that cells with +TMPRSS2 are over-expressing TMPRSS2 while cells with -TMPRSS2 have had TMPRSS2 knocked out. Bottom figure shows the distributions of fusion rate estimates for the different Vero/293 combinations (left) and the different 293/Vero combinations (right).

(1.79–3.50) × 10^{-3}/h) when acceptor cells over-express TMPRSS2 and a fusion rate of 1.23×10^{-3}/h (95% CI (0.713–2.15) × 10^{-3}/h) when the acceptor cells have TMPRSS2 knocked out. For the 293/Vero combination, we find a fusion rate of 3.96×10^{-3}/h (95% CI (2.88–7.47) × 10^{-3}/h). For cells over-expressing TMPRSS2, we find a statistically significant increase in the fusion rate for both donor/acceptor combinations ($p < 1\times10^{-3}$ for both cell combinations). In the case of the TMPRSS2 knockout cells, we find a higher fusion rate than baseline, although the difference is not statistically significant ($p = 0.081$).

3.3. Effect of furin

Experiments to study the effect of furin were performed with a single donor/acceptor combination (293/Vero), but furin knockouts were created for both Vero and 293 cells to study whether it is the presence of furin on the donor or acceptor cells that affects the fusion rate. Fig. 3 shows the experimental time courses of the data sets used in this analysis along with model best fits. The estimated fusion rate distributions are shown in the bottom row of Fig. 3. Best fit parameter estimates are given in Table 4 while correlation plots and likelihood profiles are given in the Supplementary Material.

The fusion rate for the 293/Vero combination without any changes to furin expression is 6.85×10^{-4}/h (6.04–7.63) × 10^{-4}/h). When furin is removed from the acceptor cells, we find a statistically significant ($p < 0.001$) higher fusion rate of 1.03×10^{-3}/h (95% CI (0.818–1.23) × 10^{-3}/h), indicating that removal of furin on the acceptor does not cause inhibition of fusion. On the other hand, removal of furin on the donor cells causes a statistically significant ($p < 0.001$) decrease in the fusion rate to 4.98×10^{-4}/h (95% CI (4.64–5.28) × 10^{-4}/h). Removing furin from both donor and acceptor cells causes the largest decrease in the fusion rate to 2.08×10^{-4}/h (95% CI (1.46 × 10^{-4}–12×10^{-4}/h3-2.68) × 10^{-4}/h).

Table 4
Best fit parameter values for experiments examining the effect of furin.

Experiment	Fusion rate (/hour)	Initial percentage of donors	SSR
293/Vero	6.85 (6.04–7.63)× 10^{-4}	62.7 (60.8–64.7)	56.6 (19.7–88.4)
293/Vero-furin	1.03 (0.818–1.23)× 10^{-3}	65.2 (63.3–67.6)	129 (22.1–223)
293-furin/Vero	4.98 (4.64–5.28)× 10^{-4}	5.68 (90.4–93.1)	15.4 (4.84–21.3)
293-furin/Vero-furin	2.08 (1.43–2.68)× 10^{-4}	13.0 (8.63–22.9)	11.9 (2.36–19.5)

3.4. Availability of the spike cleavage site

In the previous sections, we examined the effect of changing expression of proteases on the donor and acceptor cells. In no case was fusion completely blocked since furin and TMPRSS2 were individual changed, leaving the other protease unaffected. In a further attempt to study the role of cleavage of the spike protein in syncytia formation, the cleavage site on the spike protein was changed, which prevents proteases from easily cleaving the protein. Fig. 4 shows the experimental time courses of the data sets used in this analysis along with model best fits. The estimated fusion rate distributions are shown in the bottom row of Fig. 4. Best fit parameter estimates are given in Table 5 while correlation plots and likelihood profiles are given in the Supplementary Material.

There is a very clear drop in the fusion rate when the spike cleavage site is altered, going from 6.85×10^{-4}/h (95% CI (6.04–7.63) × 10^{-4}/h) at baseline to 6.45×10^{-5}/h (95% CI (4.79–22.1) × 10^{-5}/h) when the cleavage site is removed ($p < 0.001$). The removal of furin on either the donors or acceptors, or both, does not further decrease the fusion rate, suggesting that the presence or absence of furin is not relevant once the

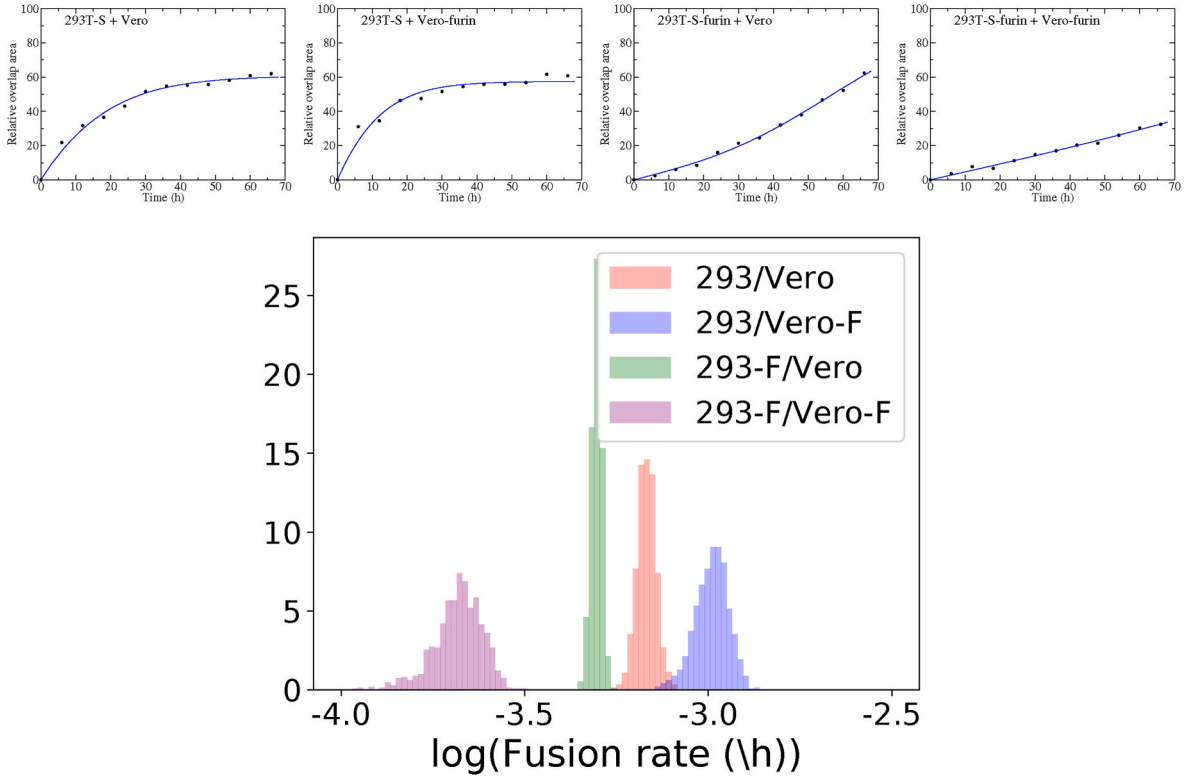

Fig. 3. Dependence of fusion rate estimates on furin. Top row shows the experimental time courses of (from left to right) 293/Vero fusion, 293/Vero-furin fusion, 293-furin/Vero, and 293-furin/Vero-furin, along with model best fit curves. Bottom figure shows the distributions of fusion rate estimates for the different 293/Vero combinations.

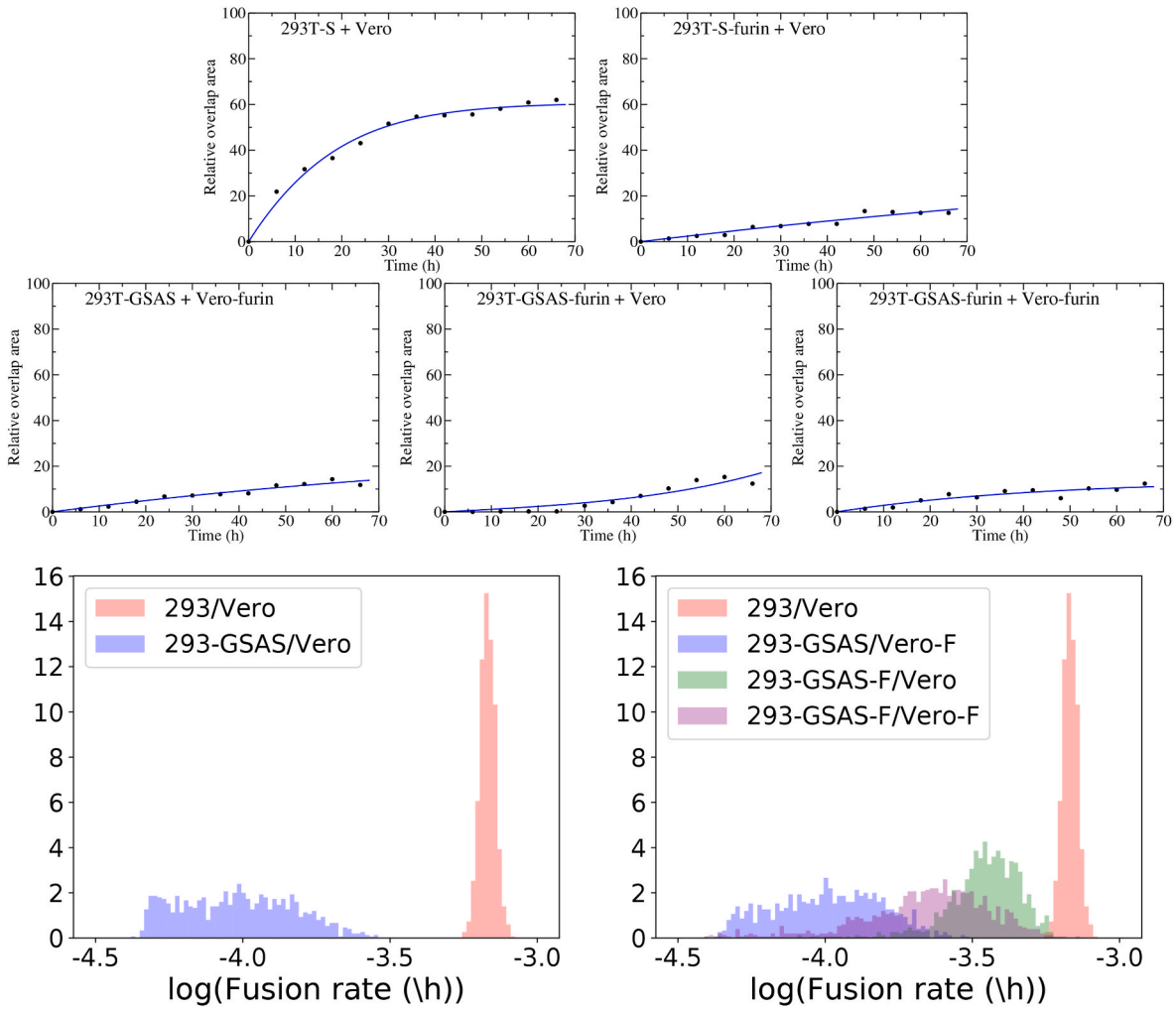

Fig. 4. Dependence of fusion rate estimates on availability of the cleavage site. Top row shows the experimental time courses of (left) 293/Vero fusion and (right) 293-GSAS/Vero fusion time courses along with model best fit curves. The center row shows (left) 293-GSAS/Vero-furin fusion, (center) 293-GSAS-furin/Vero fusion, and (right) 293-GSAS-furin/Vero-furin fusion time courses along with model best fit curves. Bottom figures show the distributions of fusion rate estimates for (left) 293/Vero with and without the altered spike protein and (right) with altered spike protein and furin knockout cells.

Table 5
Best fit parameter values for experiments examining the effect of changing the spike protein cleavage site.

Experiment	Fusion rate (/hour)	Initial percentage of donors	SSR
293/Vero	6.85 (6.04–7.63)×10^{-4}	62.7 (60.8–64.7)	56.6 (19.7–88.4)
293-GSAS/Vero	6.45 (4.79–22.1)×10^{-5}	74.3 (5.23–90.8)	16.6 (3.13–26.0)
293-GSAS/Vero-furin	9.86 (4.82–21.7)×10^{-5}	83.8 (9.95–91.3)	11.1 (3.09–16.9)
293-GSAS-furin/Vero	3.95 (1.70–5.42)×10^{-4}	1.40 (0.624–6.17)	49.1 (14.6–69.8)
293-GSAS-furin/Vero-furin	2.38 (0.648–4.89)×10^{-4}	92.8 (74.6–94.8)	22.2 (4.94–39.4)

Table 6
Best fit parameter values for experiments examining the effect of changing the spike protein cleavage site.

Experiment	Fusion rate (/hour)	Initial percentage of donors	SSR
Vero/293	6.33 (5.60–8.98)×10^{-4}	26.0 (11.5–49.4)	160 (19.7–236)
Vero-GSAS/293	5.80 (1.27–13.4)×10^{-4}	95.3 (85.1–96.6)	9.03 (1.06–14.6)
Vero-GSAS/293-TMPRSS2	1.71 (1.09–19.1)×10^{-5}	20.0 (1.37–92.7)	0.239 (0.0326–0.411)

cleavage site is removed.

A similar set of experiments was performed for the Vero/293 combination, although in this case, TMPRSS2 rather than furin was removed from the acceptor cells. Fig. 5 shows the experimental time courses of the data sets used in this analysis along with model best fits. The estimated fusion rate distributions are shown in the bottom row of Fig. 5. Best fit parameter estimates are given in Table 6, while correlation plots and likelihood profiles are given in the Supplementary Material.

When the donor and acceptor cells are switched, there isn't a statistically significant change in the fusion rate when the cleavage site is altered ($p = 0.42$). We find a fusion rate of 6.33×10^{-4}/h (95% CI (5.60–8.98) $\times$ 10^{-4}/h) with the unaltered cleavage site and a fusion rate of 5.80×10^{-4}/h (95% CI (1.27–13.4) $\times$ 10^{-4}/h) when the cleavage site is altered. However, when TMPRSS2 is removed acceptor cells, there is a statistically significant change in the fusion rate ($p < 0.001$), falling to 1.71×10^{-5}/h (95% CI (1.09–19.1) $\times$ 10^{-5}/h).

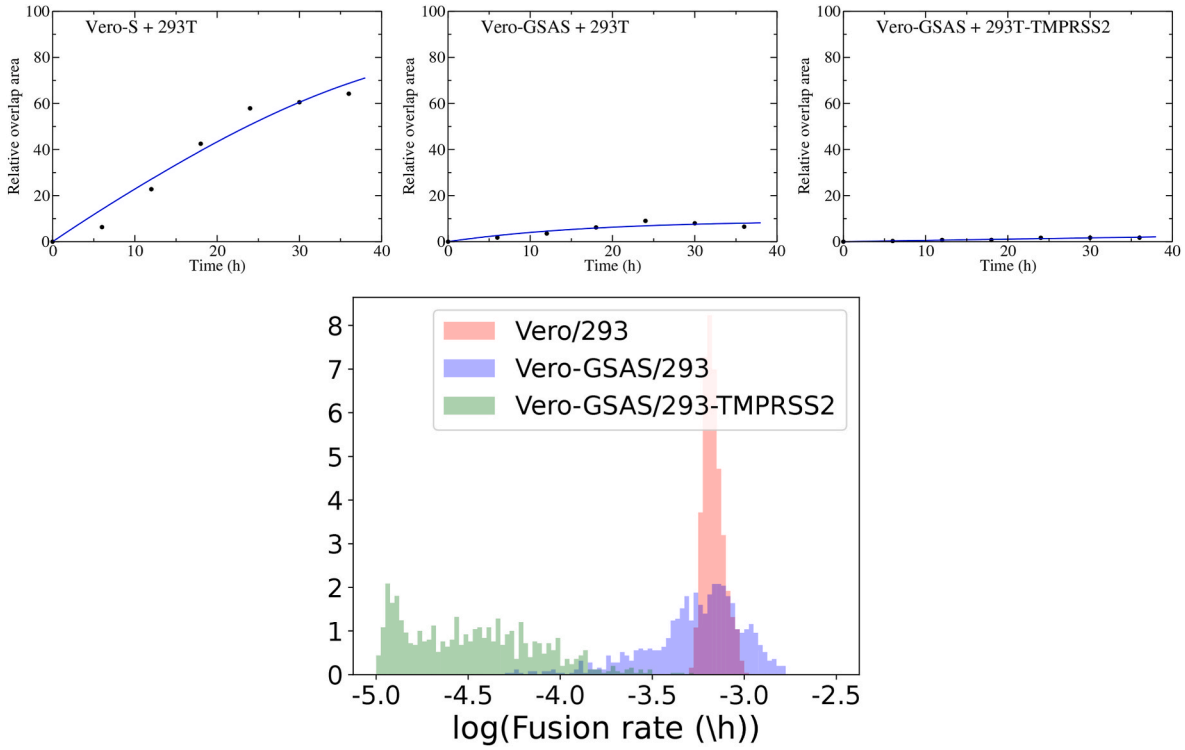

Fig. 5. Dependence of fusion rate estimates on availability of cleavage site. Top row shows the experimental time courses of (left) Vero/293 fusion, (center) Vero-GSAS/293, and (right) Vero-GSAS/293-TMPRSS2 fusion time courses along with model best fit curves. Bottom figure shows the distributions of fusion rate estimates for altered spike protein and TMPRSS2 knockout cells.

4. Discussion

We used mathematical modeling to estimate the virus-mediated cell fusion rate of SARS-CoV-2. To our knowledge, the virus-mediated cell fusion rate has not been estimated for any virus, even though cell-cell fusion assays have been performed for a number of other syncytia-forming viruses (Pare et al., 2005; Marin et al., 2015; Kobayashi et al., 2006; Claus et al., 2006). In this manuscript, we have shown that by applying a simple mathematical model, more quantitative information can be gleaned from these types of biological assays, provided measurements are taken at multiple time points. Viruses that are known to form syncytia include varicella-zoster virus (responsible for chicken pox and shingles) (Wang et al., 2017), rotavirus (Diller et al., 2019), human immunodeficiency virus (Symeonides et al., 2015), other coronaviruses (responsible for Middle East respiratory syndrome (MERS) and severe acute respiratory syndrome (SARS)) (Qian et al., 2013; Buchrieser et al., 2020), measles (Ayata et al., 2007), and respiratory syncytial virus (Saleh et al., 2020; Domachowske et al., 2000). The ability to quantify the fusion rate of these viruses under different conditions could lead to a better understanding of why the formation of syncytia might be beneficial to spread of the virus.

In addition to simply estimating the virus-mediated cell fusion rate, we were able to compare fusion rates of SARS-CoV-2 under different conditions. We found that overexpression of the protease TMPRSS2 at least doubled the fusion rate, however, knocking out TMPRSS2 did not lower the fusion rate. This could be because there is an alternative fusion pathway via furin, so removal of only one of the proteases does not slow down the fusion process. When examining experiments that eliminated furin, we found that removing furin on the donor cells lowered the fusion rate by about 30%, but that removing furin from the acceptor cells nearly doubled the fusion rate. This is an unusual result for which we have no explanation, particularly since removal of furin from both donor and acceptor cells decreased the fusion rate more (by 70%) than removing furin from the donor cells only. Finally, alteration of the spike protein cleavage site reduced the fusion rate by a factor of 10 when 293 cells were the donor cells, but not when the Vero cells were the donor. However, when TMPRSS2 was removed from the corresponding acceptor cells, the fusion rate dropped, suggesting that the altered spike protein could still potentially be cleaved by TMPRSS2. While these conclusions are in line with the conclusions reached by Papa et al. (2021), our modeling methodology allows us to quantify the changes in fusion rate, rather than simply stating that fusion decreased or increased.

This type of cell-cell fusion assay has previously been used to assess the effect of antivirals (Marin et al., 2015; Ji et al., 2006, 2007; Wang et al., 2020; Torriani et al., 2019), specifically those that target viral entry or fusion. For assessment of antivirals, the cell-cell fusion assay is performed with varying concentrations of the antiviral and measurement of the amount of fusion at a particular time is measured to create a dose-response curve. Unfortunately the drug effectiveness characterized by these types of measurements are dependent on the measurement time (Murphy et al., 2020). Using changes in the fusion rate could provide a more consistent characterization of the antiviral effect, similar to the suggested use of changes in growth rate to characterize the effect of anti-cancer drugs (Hafner et al., 2016; Harris et al., 2016).

In order to use this methodology for drug characterization, we will need to ensure that we can consistently make accurate estimates of the fusion rate. While we found that the estimated fusion rate was quite consistent between different model fits for the 66 h data sets, we noted that there was variation in fusion rate estimates that depended on fitting or model details for the shorter, 36 h data sets (Supplementary Material). Thus, it's clear that data must be taken over a sufficiently long time period, although we have not identified a minimum length of time here. We also noted that there might be an issue with reproducibility of the actual cell-cell fusion assays by comparing fusion estimates from different experiments using the same donor and acceptor cells (see Supplementary Material). A similar reproducibility problem has been noted for single cycle and multiple cycle virus growth assays (Paradis

et al., 2015).

An additional factor that was not taken into account in the models was possible replication of the donor and/or acceptor cells. In the fits assuming 100% coverage, additional cell division is not possible, but in the fits assuming less than 100% coverage, cell replication could potentially be considered. Vero cells double every 24 h or so (Nahapetian et al., 1986) and 293T cells divide every 12–20 h (Thomas and Smart, 2005) under ideal conditions, so even in the 36 h data sets, we might expect some cell replication. Including cell replication would require addition of a logistic growth term (Verhulst, 1838) for both donor and acceptor cells. The carrying capacity is known, but the growth rates of both donor and acceptor cells are additional free parameters that need to be determined through fitting. Perhaps if we had measurements of donor and acceptor cell time courses, along with measurements of the syncytia time course, it would make sense to incorporate these additional details.

The model also assumes that fusion happens instantaneously when in reality it is a multi-step process that requires a finite amount of time (Borkotoky et al., 2021). A more recent cell-cell fusion assay examining syncytia formation in different SARS-CoV-2 variants took more frequent measurements during the experiment (Rajah et al., 2021). Their data shows a clear delay in the onset of syncytia formation lasting about 4 h after donor/acceptor plating. Note that the first measurement in all the Papa et al. data sets is at 6 h, so this delay is missed due to the sparse sampling of the data. Such a delay can be incorporated into the mathematical model by adding a "fusing" state between the unfused donors/acceptors and the syncytia.

Another drawback to the methodology used here is the well-mixed assumption underlying ordinary differential equations (ODEs). If the donor and acceptor cells are plated at near 50/50 and are well-mixed, then the ODE approximation is probably reasonable, at least in the early stages of the experiment. Although cells are only interacting with their nearest neighbours, each donor should have access to an acceptor. Once large syncytia have formed, the well-mixed assumption breaks down since some of the area covered by cells now fused into the syncytia is surrounded by syncytia and does not have access to donor or acceptor cells. This is no longer a well-mixed scenario. Additionally, if the initial ratio of donor to acceptor is skewed away from 50/50 or if they are not well-mixed before plating, the ODE framework also breaks down. In these scenarios, there are likely to be patches of donor cells or patches of acceptor cells such that some donor or acceptor cells are entirely surrounded by cells of the same type and cannot fuse. This inherent spatial heterogeneity might be the reason that the asymmetric model provides somewhat better fits to the data. When the mix of donors and acceptors is near 50/50, correlation plots (Supplementary Material) suggest that the estimated fusion rates are independent of the initial fraction of donors. Many of the model fits here tended towards small or high initial fractions of donors, perhaps to help account for spatial heterogeneity. Future experiments should try to ensure an equal distribution of donors and acceptors so that ODE models can be used, or mathematical models incorporating spatial heterogeneity, such as agent-based models (Fain and Dobrovolny, 2022), should be used to provide better parameter estimates.

While there are still possible improvements that can be made to the methodology, this manuscript presents a novel mathematical model of cell-cell fusion assays that can estimate the virus-mediated cell fusion rate. We applied the model to data from SARS-CoV-2 cell fusion assays to provide the first estimates of SARS-CoV-2 fusion rate under various conditions.

CRediT authorship contribution statement

Ava Amidei: Methodology, Software, Validation, Formal analysis, Data curation, Writing – review & editing, Visualization, Supervision, Project administration, All authors have read, and agreed to the published version of the manuscript. **Hana M. Dobrovolny:** Conceptualization, Methodology, Validation, Formal analysis, Writing – original draft, preparation, Writing – review & editing, Visualization, Supervision, Project administration.

Declaration of competing interest

The authors declare that they have no known competing financial interests or personal relationships that could have appeared to influence the work reported in this paper.

Appendix A. Supplementary data

Supplementary data to this article can be found online at https://doi.org/10.1016/j.virol.2022.08.016.

References

Acer, O., Bahce, Y.G., Ozudogru, O., 2022. Association of viral load with age, gender, disease severity, and death in severe acute respiratory syndrome coronavirus 2 variants. J. Med. Virol. 94 (7), 3063–3069. https://doi.org/10.1002/jmv.27677.

Alzahrani, T., Eftimie, R., Trucu, D., 2020. Multiscale moving boundary modelling of cancer interactions with a fusogenic oncolytic virus: the impact of syncytia dynamics. Math. Biosci. 323, 108296 https://doi.org/10.1016/j.mbs.2019.108296.

Ayata, M., Shingai, M., Ning, X., Matsumoto, M., Seya, T., Otani, S., Seto, T., Ohgimoto, S., Ogura, H., 2007. Effect of the alterations in the fusion protein of measles virus isolated from brains of patients with subacute sclerosing panencephalitis on syncytium formation. Virol. Res. 130 (1–2), 260–268. https://doi.org/10.1016/j.virusres.2007.07.017.

Baccam, P., Beauchemin, C., Macken, C.A., Hayden, F.G., Perelson, A.S., 2006. Kinetics of influenza A virus infection in humans. J. Virol. 80 (15), 7590–7599. https://doi.org/10.1128/JVI.01623-05.

Barreto-Vieira, D.F., da Silva, M.A.N., de Almeida, A.L.T., da Costa Rasinhas, A., Monteiro, M.E., Miranda, M.D., Motta, F.C., Siqueira, M.M., Girard-Dias, W., Archanjo, B.S., Bozza, P.T., Souza, T.M.L., Gomes Dias, S.S., Soares, V.C., Barth, O. M., 2022. SARS-CoV-2: ultrastructural characterization of morphogenesis in an in vitro system. Viruses 14 (2), 201. https://doi.org/10.3390/v14020201.

Borkotoky, S., Dey, D., Banerjee, M., 2021. Computational insight into the mechanism of SARS-CoV-2 membrane fusion. J. Chem. Inf. Model. 61 (1), 423–431. https://doi.org/10.1021/acs.jcim.0c01231.

Braga, L., Ali, H., Secco, I., Chiavacci, E., Neves, G., Goldhill, D., Penn, R., Jimenez-Guardeno, J.M., Ortega-Prieto, A.M., Bussani, R., Cannata, A., Rizzari, G., Collesi, C., Schneider, E., Arosio, D., Shah, A.M., Barclay, W.S., Malim, M.H., Burrone, J., Giacca, M., 2021. Drugs that inhibit TMEM16 proteins block SARS-CoV-2 spike-induced syncytia. Nature 594 (7861), 88. https://doi.org/10.1038/s41586-021-03491-6.

Buchrieser, J., Dufloo, J., Hubert, M., Monel, B., Planas, D., Rajah, M.M., Planchais, C., Porrot, F., Guivel-Benhassine, F., der Werf, S.V., Casartelli, N., Mouquet, H., Bruel, T., Schwartz, O., 2020. Syncytia formation by sars-cov-2 infected cells. EMBO J. 39 (23), e106267 https://doi.org/10.15252/embj.2020106267.

Bussani, R., Schneider, E., Zentilin, L., Collesi, C., Ali, H., Braga, L., Volpe, M.C., Colliva, A., Zanconati, F., Berlot, G., Silvestri, F., Zacchigna, S., Giacca, M., 2020. Persistence of viral RNA, pneumocyte syncytia and thrombosis are hallmarks of advanced COVID-19 pathology. eBiomed 61, 103104. https://doi.org/10.1016/j.ebiom.2020.103104.

Chen, N., Zhou, M., Dong, X., Qu, J., Gong, F., Han, Y., Qiu, Y., Wang, J., Liu, Y., Wei, Y., Xia, J., Yu, T., Zhang, X., Zhang, L., 2020. Epidemiological and clinical characteristics of 99 cases of 2019 novel coronavirus pneumonia in Wuhan, China: a descriptive study. Lancet 395 (10223), 507–513. https://doi.org/10.1016/S0140-6736(20)30211-7.

Claus, C., Hofmann, J., Uberla, K., Liebert, U., 2006. Rubella virus pseudotypes and a cell-cell fusion assay as tools for functional analysis of the rubella virus E2 and E1 envelope glycoproteins. J. Gen. Virol. 87, 3029–3037. https://doi.org/10.1099/vir.0.82035-0.

Diller, J.R., Parrington, H.M., Patton, J.T., Ogden, K.M., 2019. Rotavirus species B encodes a functional fusion-associated small transmembrane protein. J. Virol. 93 (20) https://doi.org/10.1128/JVI.00813-19 e00813–19.

Dobrovolny, H.M., 2020. Quantifying the effect of remdesivir in rhesus macaques infected with SARS-CoV-2. Virol 550, 61–69. https://doi.org/10.1016/j.virol.2020.07.015.

Domachowske, J., Bonville, C., Rosenberg, H., 2000. Cytokeratin 17 is expressed in cells infected with respiratory syncytial virus via NF-kappa B activation and is associated with the formation of cytopathic syncytia. J. Infect. Dis. 182 (4), 1022–1028. https://doi.org/10.1086/315841.

Efron, B., Tibshirani, R., 1986. Bootstrap methods for standard errors, confidence intervals, and other measures of statistical accuracy. Stat. Sci. 1 (1), 54–75.

El Jamal, S.M., Pujadas, E., Ramos, I., Bryce, C., Grimes, Z.M., Amanat, F., Tsankova, N. M., Mussa, Z., Olson, S., Salem, F., Miorin, L., Aydillo, T., Schotsaert, M., Albrecht, R. A., Liu, W.-C., Marjanovic, N., Francoeur, N., Sebra, R., Sealfon, S.C., Garcia-Sastre, A., Fowkes, M., Cordon-Cardo, C., Westra, W.H., 2021. Tissue-based SARS-CoV-2 detection in fatal COVID-19 infections: sustained direct viral-induced damage

is not necessary to drive disease progression. Hum. Pathol. 114, 110–119. https://doi.org/10.1016/j.humpath.2021.04.012.
Fain, B., Dobrovolny, H.M., 2022. GPU acceleration and data fitting: agent-based models of viral infections can now be parameterized in hours. J. Comput. Sci. 61, 101662 https://doi.org/10.1016/j.jocs.2022.101662.
González-Parra, G., Dobrovolny, H.M., 2015. Assessing uncertainty in A2 respiratory syncytial virus viral dynamics, 2015 Comput. Math. Methods Med., 567589. https://doi.org/10.1155/2015/567589.
González-Parra, G., Dobrovolny, H.M., 2018. A quantitative assessment of dynamical differences of RSV infections in vitro and in vivo. Virol 523, 129–139. https://doi.org/10.1016/j.virol.2018.07.027.
González-Parra, G., Dobrovolny, H.M., Aranda, D.F., Chen-Charpentier, B., Roja, R.A.G., 2018. Quantifying rotavirus kinetics in the REH tumor cell line using in vitro data. Virus Res. 244, 53–63. https://doi.org/10.1016/j.virusres.2017.09.023.
Goyal, P., Choi, J.J., Pinheiro, L.C., Schenck, E.J., Chen, R., Jabri, A., Satlin, M.J., Campion, T.R., Nahid, M., Ringel, J.B., Hoffman, K.L., Alshak, M.N., Li, H.A., Wehmeyer, G.T., Rajan, M., Reshetnyak, E., Hupert, N., Horn, E.M., Martinez, F.J., Gulick, R.M., Safford, M.M., 2020. Clinical characteristics of COVID-19 in New York City. N. Engl. J. Med. 382, 2372–2374. https://doi.org/10.1128/JVI.00689-10.
Hafner, M., Niepel, M., Chung, M., Sorger, P.K., 2016. Growth rate inhibition metrics correct for confounders in measuring sensitivity to cancer drugs. Nat. Methods 13 (6), 521. https://doi.org/10.1038/NMETH.3853.
Hakim, A., Hasan, M.M., Hasan, M., Lokman, S.M., Azim, K.F., Raihan, T., Chowdhury, P. A., Azad, A.K., 2021. Major insights in dynamics of host response to SARS-CoV-2: impacts and challenges. Front. Microbiol. 12, 637554 https://doi.org/10.3389/fmicb.2021.637554.
Harris, L.A., Frick, P.L., Garbett, S.P., Hardeman, K.N., Paudel, B.B., Lopez, C.F., Quaranta, V., Tyson, D.R., 2016. An unbiased metric of antiproliferative drug effect in vitro. Nat. Methods 13 (6), 497–502. https://doi.org/10.1038/nMeth.3852.
Hernandez-Vargas, E.A., Velasco-Hernandez, J.X., 2020. In-host modelling of COVID-19 kinetics in humans, 2020 Annu. Rev. Control 50, 448–456. https://doi.org/10.1101/2020.03.26.20044487.
Hoernich, B.F., Grosskopf, A.K., Schlagowski, S., Tenbusch, M., Kleine-Weber, H., Neipel, F., Stahl-Hennig, C., Hahn, A.S., 2021. SARS-CoV-2 and SARS-CoV spike-mediated cell-cell fusion differ in their requirements for receptor expression and proteolytic activation. J. Virol. 95 (9) https://doi.org/10.1128/JVI.00002-21 e00002–21.
Hoffmann, M., Kleine-Weber, H., Pohlmann, S., 2020. A multibasic cleavage site in the spike protein of SARS-CoV-2 is essential for infection of human lung cells. Mol. Cell 78 (4), 779–784. https://doi.org/10.1016/j.molcel.2020.04.022.
Jessie, B., Dobrovolny, H., 2021. The role of syncytia during viral infections. J. Theor. Biol. 525, 110749 https://doi.org/10.1016/j.jtbi.2021.110749.
Ji, C., Jun, Z., Cammack, N., Sankuratri, S., 2006. Development of a novel dual CCR5-dependent and CXCR4-dependent cell-cell fusion assay system with inducible gp160 expression. J. Biomol. Screen 11 (1), 65–74. https://doi.org/10.1177/1087057105282959.
Ji, C., Zhang, J., Dioszegi, M., Chiu, S., Rao, E., deRosier, A., Cammack, N., Brandt, M., Sankuratri, S., 2007. CCR5 small-molecule antagonists and monoclonal antibodies exert potent synergistic antiviral effects by cobinding to the receptor. Mol. Pharmacol. 72 (1), 18–28. https://doi.org/10.1124/mol.107.035055.
S. A. Khan, K. Zia, S. Ashraf, R. Uddin, Z. Ul-Haq, Identification of chymotrypsin-like proteaseinhibitors of SARS-CoV-2 via integratedcomputational approach, J. Biomol. Struct. Dyn.doi:10.1080/07391102.2020.1751298.
Jiang, F., Deng, L., Zhang, L., Cai, Y., Cheung, C.W., Xia, Z., 2020. Review of the clinical characteristics of coronavirus disease 2019 (COVID-19). J. Gen. Intern. Med. 34, 1545–1549. https://doi.org/10.1007/s11606-020-05762-w.
Kobayashi, M., Bennett, M., Bercot, T., Singh, I., 2006. Functional analysis of hepatitis C virus envelope proteins, using a cell-cell fusion assay. J. Virol. 80 (4), 1817–1825. https://doi.org/10.1128/JVI.80.4.1817-1825.2006.
Liao, L.E., Carruthers, J., Smither, S.J., Weller, S.A., Williamson, D., Laws, T.R., Garcia-Dorival, I., Hiscox, J., Holder, B.P., Beauchemin, C.A., Perelson, A.S., Lopez-Garcia, M., Lythe, G., Barr, J.N., Molina-Paris, C., 2020. Quantification of Ebola virus replication kinetics in vitro. PLoS Comput. Biol. 16 (11), e1008375 https://doi.org/10.1371/journal.pcbi.1008375.
Marin, M., Du, Y., Giroud, C., Kim, J.H., Qui, M., Fu, H., Melikyan, G., 2015. High-throughput HIV-cell fusion assay for discovery of virus entry inhibitors. Assay Drug Dev. Technol. 13 (3), 155–166. https://doi.org/10.1089/adt.2015.639.
Murphy, H., McCarthy, G., Dobrovolny, H.M., 2020. Understanding the effect of measurement time on drug characterization. PLoS One 15 (5), e0233031. https://doi.org/10.1371/journal.pone.0233031.
Nahapetian, A., Thomas, J., Thilly, W., 1986. Optimization of environment for high-density Vero cell-culture — effect of dissolved-oxygen and nutrient supply on cell-growth and changes in metabolites. J. Cell Sci. 81, 65–103.
Papa, G., Mallery, D.L., Albecka, A., Welch, L.G., Cattin-Ortola, J., Luptak, J., Paul, D., McMahon, H.T., Goodfellow, I.G., Carter, A., Munro, S., James, L.C., 2021. Furin cleavage of SARS-CoV-2 spike promotes but is not essential for infection and cell-cell fusion. PLoS Pathog. 17 (1), e1009246 https://doi.org/10.1371/journal.ppat.1009246.
Paradis, E., Pinilla, L., Holder, B., Abed, Y., Boivin, G., Beauchemin, C., 2015. Impact of the H275Y and I223V mutations in the neuraminidase of the 2009 pandemic influenza virus in vitro and evaluating experimental reproducibility. PLoS One 10 (5), e0126115. https://doi.org/10.1371/journal.pone.0126115.
Pare, M., Gauthier, S., Landry, S., Sun, J., Legault, E., Leclerc, D., Tanaka, Y., Marriott, S., Tremblay, N., Barbeau, B., 2005. A new sensitive and quantitative HTLV-I-mediated cell fusion assay in T cells. Virol 338 (2), 309–322. https://doi.org/10.1016/j.virol.2005.05.012.
Petrie, S.M., Butler, J., Barr, I.G., McVernon, J., Hurt, A.C., McCaw, J.M., 2015. Quantifying relative within-host replication fitness in influenza virus competition experiments. J. Theor. Biol. 382, 259–271. https://doi.org/10.1016/j.jtbi.2015.07.003.
Pinilla, L.T., Holder, B.P., Abed, Y., Boivin, G., Beauchemin, C.A.A., 2012. The H275Y neuraminidase mutation of the pandemic A/H1N1 influenza virus lengthens the eclipse phase and reduces viral output of infected cells, potentially compromising fitness in ferrets. J. Virol. 86 (19), 10651–10660. https://doi.org/10.1128/JVI.07244-11.
Qian, Z., Dominguez, S.R., Holmes, K.V., 2013. Role of the spike glycoprotein of human middle east respiratory syndrome coronavirus (MERS-CoV) in virus entry and syncytia formation. PLoS One 8 (10), e76469. https://doi.org/10.1371/journal.pone.0076469.
Rajah, M.M., Hubert, M., Bishop, E., Saunders, N., Robinot, R., Grzelak, L., Planas, D., Dufloo, J., Gellenoncourt, S., Bongers, A., Zivaljic, M., Planchais, C., Guivel-Benhassine, F., Porrot, F., Mouquet, H., Chakrabarti, L.A., Buchrieser, J., Schwartz, O., 2021. SARS-CoV-2 alpha, beta, and delta variants display enhanced spike-mediated syncytia formation. EMBO J. 40 (24), e108944 https://doi.org/10.15252/embj.2021108944.
Ren, H., Ma, C., Peng, H., Zhang, B., Zhou, L., Su, Y., Gao, X., Huang, H., 2021. Micronucleus production, activation of DNA damage response and cGAS-STING signaling in syncytia induced by SARS-CoV-2 infection. Biol. Direct 16 (1), 20. https://doi.org/10.1186/s13062-021-00305-7.
Rezelj, V.B. ad Veronica V., Vignuzzi, M., 2020. Modelling degradation and replication kinetics of the zika virus in vitro infection. Viruses 12 (5), 547.
Rodriguez, T., Dobrovolny, H.M., 2021. Estimation of viral kinetics model parameters in young and aged SARS-CoV-2 infected macaques. R. Soc. Open Sci. 8, 202345 https://doi.org/10.1098/rsos.202345.
Saleh, F., Harb, A., Soudani, N., Zaraket, H., 2020. A three-dimensional A549 cell culture model to study respiratory syncytial virus infections. J. Infect. Pub. Health 13 (8), 1142–1147. https://doi.org/10.1016/j.jiph.2020.03.011.
Sanders, D.W., Jumper, C.C., Ackerman, P.J., Bracha, D., Donlic, A., Kim, H., Kenney, D., Castello-Serrano, I., Suzuki, S., Tamura, T., Tavares, A.H., Saeed, M., Holehouse, A. S., Ploss, A., Levental, I., Douam, F., Padera, R.F., Levy, B.D., Brangwynne, C.P., 2021. SARS-CoV-2 requires cholesterol for viral entry and pathological syncytia formation. Elife 10, e65962. https://doi.org/10.7554/eLife.65962.
Simon, P.F., de La Vega, M.-A., Paradis, É., Mendoza, E., Coombs, K.M., Kobasa, D., Beauchemin, C.A.A., 2016. Avian influenza viruses that cause highly virulent infections in humans exhibit distinct replicative properties in contrast to human H1N1 viruses. Sci. Rep. 6, 24154 https://doi.org/10.1038/srep24154.
Simons, L.M., Lorenzo-Redondo, R., Gibson, M., Kinch, S.L., Vandervaart, J.P., Reiser, N. L., Eren, M., Lux, E., McNally, E., Tambur, A.R., Vaughan, D.E., Bachta, K.E., Demonbreun, A.R., Satchell, K.J., Achenbach, C.J., Ozer, E.A., Ison, M.G., Hultquist, J.F., 2022. Assessment of virological contributions to COVID-19 outcomes in a longitudinal cohort of hospitalized adults. Open Forum Infect. Dis. 9 (3) https://doi.org/10.1093/ofid/ofac027 ofac027.
Sun, L., Shen, L., Fan, J., Gu, F., Hu, M., An, Y., Zhou, Q., Fan, H., Bi, J., 2020. Clinical features of patients with coronavirus disease 2019 from a designated hospital in Beijing, China. J. Med. Virol. 92 (10), 2055–2066. https://doi.org/10.1002/jmv.25966.
Syangtan, G., Bista, S., Dawadi, P., Rayamajhee, B., Shrestha, L.B., Tuladhar, R., Joshi, D. R., 2021. Asymptomatic SARS-CoV-2 carriers: a systematic review and meta-analysis. Front. Public Health 8, 587374. https://doi.org/10.3389/fpubh.2020.587374.
Symeonides, M., Murooka, T.T., Bellfy, L.N., Roy, N.H., Mempel, T.R., Thali, M., 2015. HIV-1-induced small T cell syncytia can transfer virus particles to target cells through transient contacts. Viruses 7 (12), 6590–6603. https://doi.org/10.3390/v7122959.
Takeda, M., 2022. Proteolytic activation of SARS-CoV-2 spike protein. Microbiol. Immunol. 66 (1), 15–23. https://doi.org/10.1111/1348-0421.12945.
Thomas, P., Smart, T.G., 2005. HEK293 cell line: a vehicle for the expression of recombinant proteins. J. Pharmacol. Toxicol. Methods 51 (3), 187–200. https://doi.org/10.1016/j.vascn.2004.08.014.
Torriani, G., Trofimenko, E., Mayor, J., Fedeli, C., Moreno, H., Michel, S., Heulot, M., Chevalier, N., Zimmer, G., Shrestha, N., Plattet, P., Engler, O., Rothenberger, S., Widmann, C., Kunz, S., 2019. Identification of clotrimazole derivatives as specific inhibitors of arenavirus fusion. J. Virol. 93 (6) https://doi.org/10.1128/JVI.01744-18 e01744–18.
Verhulst, P.-F., 1838. Notice sur la loi que la population poursuit dans son accroissement. Correspond. mathémat. et phys. 10, 113–121.
Wang, W., Yang, L., Huang, X., Fu, W., Pan, D., Cai, L., Ye, J., Liu, J., Xia, N., Cheng, T., Zhu, H., 2017. Outer nuclear membrane fusion of adjacent nuclei in varicella-zoster virus-induced syncytia. Virol 512, 34–38. https://doi.org/10.1016/j.virol.2017.09.002.
Wang, Y., Liu, T.-X., Wang, T.-Y., Tang, Y.-D., Wei, P., 2020. Isobavachalcone inhibits pseudorabies virus by impairing virus-induced cell-to-cell fusion. Virol. J. 17 (1), 39. https://doi.org/10.1186/s12985-020-01312-2.
Wang, X., Chen, C.-H., Badeti, S., Cho, J.H., Naghizadeh, A., Wang, Z., Liu, D., 2021. Deletion of ER-retention motif on SARS-CoV-2 spike protein reduces cell hybrid during cell-cell fusion. Cell Biosci. 11 (1), 114. https://doi.org/10.1186/s13578-021-00626-0.
wen Cheng, Y., Chao, T.-L., Li, C.-L., Wang, S.-H., Kao, H.-C., Tsai, Y.-M., Wang, H.-Y., Hsieh, C.-L., Lin, Y.-Y., Chen, P.-J., Chang, S.-Y., Yeh, S.-H., 2021. D614G substitution of SARS-CoV-2 spike protein increases syncytium formation and virus titer via enhanced furin-mediated spike cleavage. mBio 12 (4). https://doi.org/10.1128/mBio.00587-21 e00587–21.

Wethington, D., Harder, O., Uppulury, K., Stewart, W.C., Chen, P., King, T., Reynolds, S. D., Perelson, A.S., Peeples, M.E., Niewiesk, S., Das, J., 2019. Mathematical modelling identifies the role of adaptive immunity as a key controller of respiratory syncytial virus in cotton rats. J. Roy. Soc. Interface 16 (160), 20190389. https://doi.org/10.1098/rsif.2019.0389.

Wu, F., Zhao, S., Yu, B., Chen, Y.-M., Wang, W., Song, Z.-G., Hu, Y., Tao, Z.-W., Tian, J.-H., Pei, Y.-Y., Yuan, M.-L., Zhang, Y.-L., Dai, F.-H., Liu, Y., Wang, Q.-M., Zheng, J.-J., Xu, L., Holmes, E.C., Zhang, Y.-Z., 2020. A new coronavirus associated with human respiratory disease in China. Nature 579 (7798), 265–271. https://doi.org/10.1038/s41586-020-2008-3.

Zhang, Z., Zheng, Y., Niu, Z., Zhang, B., Wang, C., Yao, X., Peng, H., Franca, D.N., Wang, Y., Zhu, Y., Su, Y., Tang, M., Jiang, X., Ren, H., He, M., Wang, Y., Gao, L., Zhao, P., Shi, H., Chen, Z., Wang, X., Piacentini, M., Bian, X., Melino, G., Liu, L., Huang, H., Sun, Q., 2021a. SARS-CoV-2 spike protein dictates syncytium-mediated lymphocyte elimination. Cell Death Differ. 28 (9), 2765–2777. https://doi.org/10.1038/s41418-021-00782-3.

Zhang, L., Mann, M., Syed, Z.A., Reynolds, H.M., Tian, E., Samara, N.L., Zeldin, D.C., Tabak, L.A., Ten Hagen, K.G., 2021b. Furin cleavage of the SARS-CoV-2 spike is modulated by O-glycosylation. Proc. Natl. Acad. Sci. U.S.A. 118 (47), e2109905118 https://doi.org/10.1073/pnas.2109905118j1of7.